BIOCHEMISTRY
including biophysical chemistry & molecular biology

ARTICLE

pubs.acs.org/biochemistry

Mutations in a Helix-1 Motif of the ATP Synthase *c*-Subunit of *Bacillus pseudofirmus* OF4 Cause Functional Deficits and Changes in the *c*-Ring Stability and Mobility on Sodium Dodecyl Sulfate−Polyacrylamide Gel Electrophoresis

Jun Liu,[†] Oliver J. Fackelmayer,[†] David B. Hicks,[†] Laura Preiss,[‡] Thomas Meier,[‡] Eric A. Sobie,[†] and Terry A. Krulwich*[,†]

[†]Department of Pharmacology and Systems Therapeutics, Mount Sinai School of Medicine, 1 Gustave Levy Place, New York, New York 10029, United States

[‡]Department of Structural Biology, Max-Planck Institute of Biophysics, Max-von-Laue-Strasse 3, 60438 Frankfurt am Main, Germany

ABSTRACT: The ATP synthase of the alkaliphile *Bacillus pseudofirmus* OF4 has a tridecameric *c*-subunit rotor ring. Each *c*-subunit has an AxAxAxA motif near the center of the inner helix, where neutralophilic bacteria generally have a GxGxGxG motif. Here, we studied the impact of four single and six multiple Ala-to-Gly chromosomal mutations in the A16xAxAxA22 motif on the capacity for nonfermentative growth and, for most of the mutants, on ATP synthesis by ADP- and P_i-loaded membrane vesicles at pH 7.5 and 10.5. Sodium dodecyl sulfate−polyacrylamide gel electrophoresis (SDS−PAGE) analyses of the holo-ATP synthases were used to probe stability of the mutant *c*-rotors and mobility properties of the *c*-rotors as well as the monomeric *c*-subunits that are released from them by trichloroacetic acid treatment. Mutants containing an Ala16-to-Gly mutation exhibited the most severe functional defects. Via SDS−PAGE, most of the mutant *c*-monomers exhibited increased mobility relative to the wild-type (WT) *c*-subunit, but among the intact *c*-rings, only Ala16-to-Gly mutants exhibited significantly increased mobility relative to that of the WT *c*-ring. The hypothesis that these *c*-rings have a decreased *c*-subunit stoichiometry is still untested, but the functional impact of an Ala16-to-Gly mutation clearly depended upon additional Ala-to-Gly mutation(s) and their positions. The A16/20G double mutant exhibited a larger functional deficit than both the A16G and A16/18G mutants. Most of the mutant *c*-rings showed in vitro instability relative to that of the WT *c*-ring. However, the functional deficits of mutants did not correlate well with the extent of *c*-ring stability loss, so this property is unlikely to be a major factor in vivo.

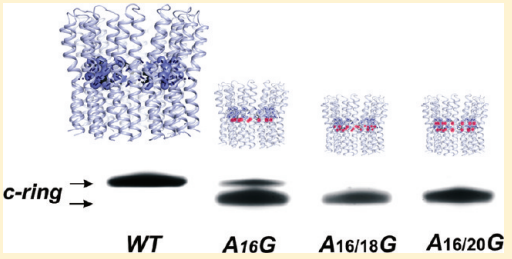

OXPHOS by the extremely alkaliphilic *Bacillus pseudofirmus* OF4 at high pH and low bulk proton-motive force (PMF) has long been hypothesized to depend upon particularly effective kinetic trapping of protons near the membrane surface as they emerge from proton-pumping respiratory chain complexes.[1] Evidence suggests that such sequestration of protons near the surface may allow protons to reach the proton-coupled F_1F_o-ATP synthase (hereafter termed ATP synthase) of alkaliphiles before they fully equilibrate with the bulk medium that can be above pH 11.[1−4] Additionally, successful function of the alkaliphile ATP synthase at high pH depends upon specific adaptations of both the respiratory chain complexes and the ATP synthase.[5−9] Adaptations of the ATP synthase to function at alkaline pH were found in the membrane-embedded F_o complex.[5,8−11] In the *c*-subunit of alkaliphiles, which forms the c_{13}-rotor ring, two specific motifs were described. The PxxExxP motif is located in the outer (C-terminal) helix and contains the conserved, proton-binding residue (Glu54 in *B. pseudofirmus* OF4).[12] The AxAxAxA motif is in the inner (N-terminal) helix of extremely alkaliphilic *B. pseudofirmus* OF4 in place of the GxGxGxG motif of most neutralophiles;[9] less extreme alkaliphiles have motifs with two or three Ala residues instead of the full four substitutions in *B. pseudofirmus* OF4[8,9] (Figure 1A). Initial studies of a panel of single, double, triple, and quadruple mutants in the alanine motif primarily focused on the quadruple mutant, which shows a major deficit in malate growth and ATP synthesis at pH 10.5; the synthetic deficits were smaller at pH 7.5, and the mutant enzyme exhibited coupled ATPase activity, with latency similar to that of the WT enzyme and sensitivity to dicyclohexylcarbodiimide inhibition.[8] We concluded that changes in the AxAxAxA motif might exert their effects via modulation of intersubunit interactions[13] that could in turn affect the pK_a of the proton-binding Glu54.[8]

In the high-resolution crystal structure of the tridecameric rotor ring of the *B. pseudofirmus* OF4 ATP synthase,[14] the overall shape of the complex was found to be slightly different from those of other rotor rings. The *B. pseudofirmus* OF4 c_{13}-ring is flared at the cytoplasmic end but more straight at the periplasmic

Received: November 5, 2010
Revised: May 10, 2011
Published: May 16, 2011

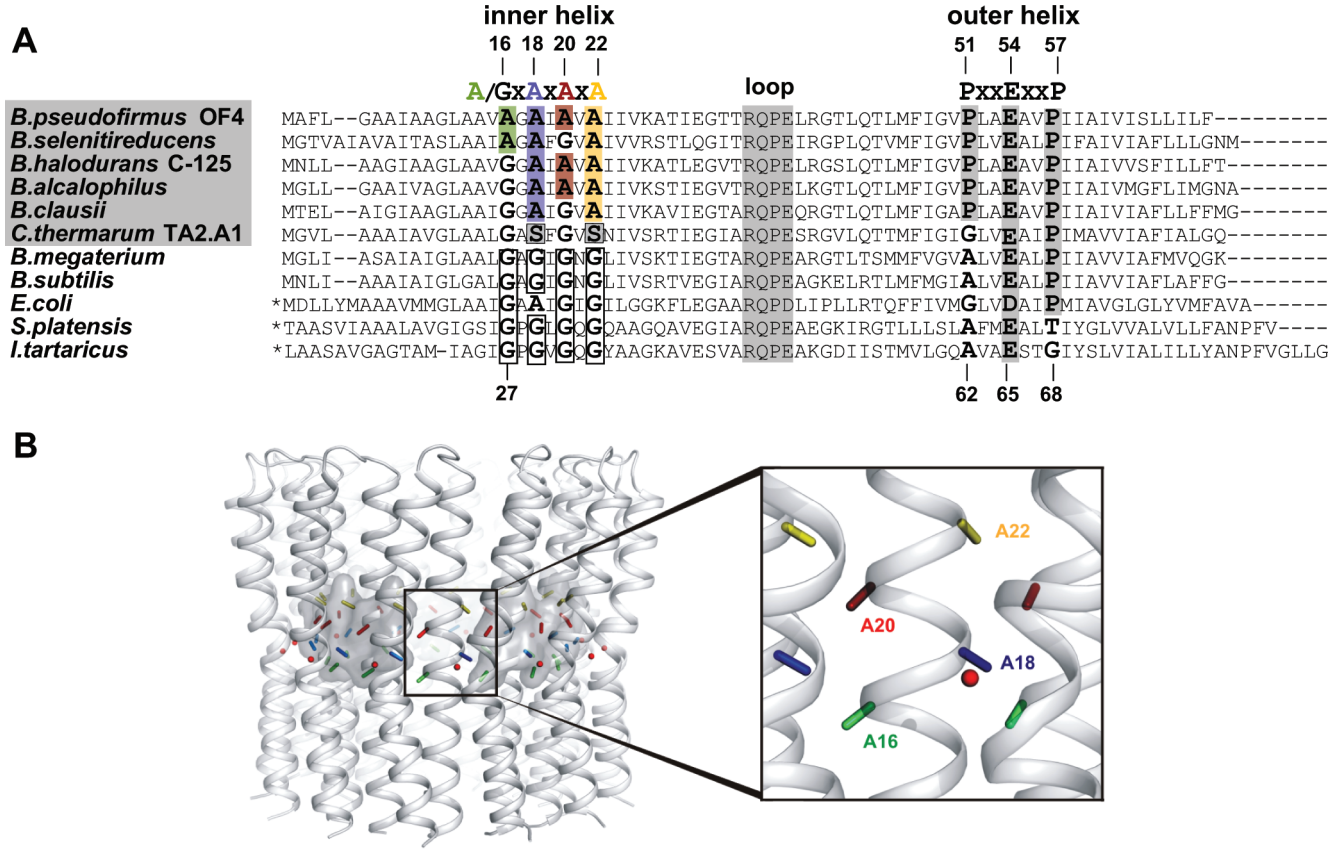

Figure 1. (A) Alignment of the *c*-subunit of the ATP synthase from several alkaliphiles and neutralophiles. The organisms shaded are the alkaliphilic *Bacillus* species. Residue numbers are given for the *B. pseudofirmus* OF4 (top) and *Ilyobacter tartaricus* *c*-subunits (bottom). The alanines of the alkaliphile AxAxAxA motif are shaded with colors corresponding to those in panel B, and PxxExxP motifs and the RQPE periplasmic loop region are shaded in gray. The two serines of a distinct thermoalkaliphile motif are shaded in gray, as they play roles in packing of the *Caldalkalibacillus thermarum* ring.[10] The open boxes show the conserved GxGxGxG motif in the inner helix of selected neutralophiles. Asterisks denote that residues were deleted from the N-terminal end of the longest *c*-subunits to maximize the size of the motif areas, 5, 6, and 10 residues from the subunits of *Escherichia coli*, *Spirulina platensis*, and *I. tartaricus*, respectively. (B) Location of the AxAxAxA motif in the *c*-ring structure of *B. pseudofirmus* OF4 as shown from the membrane plane. The four alanines are shown in different colors. The red spheres represent the bound H_2O molecules.[14] The close-up shows the *c*-ring on the level of the ion binding site perpendicular to the membrane as viewed from the cytoplasm and the alanines displayed with the same color coding.

end so that this *c*-ring lacks the pronounced hourglass shape of other high-resolution crystal structures of *c*-rings (or *K*-rings).[14−17] The shape of the c_{13}-ring reflects structural effects imposed by the AxAxAxA and PxxExxP motifs of *B. pseudofirmus* OF4 (Figure 1).[14] The AxAxAxA motif is located in the middle of the inner helix, near the ion-binding glutamate and in the area of the *c*-ring that is most tightly packed. Like the GxSxGxS motif of thermoalkaliphile *Caldalkalibacillus thermarum* TA2.A1, it is hypothesized to play a role in distancing the individual *c*-subunits from one another more than has been found in other known *c*-ring structures, thus widening the *c*-ring diameter.[10,14] Here, we examined in greater detail than in the earlier study a panel of Ala-to-Gly mutants in the alkaliphile AxAxAxA motif that includes all four single mutants, an expanded panel of four double mutants (relative to one double mutant in the earlier study), one triple mutant, and one quadruple mutant. The first major goal was to determine whether the functional impact of Ala mutations on nonfermentative growth and ATP synthase activity correlated primarily with the number of Ala-to-Gly changes in a given mutant, i.e., single, double, triple, or quadruple, or strongly depended on the positions of mutations in particular mutants. The second major goal was to take advantage of the exceptional stability of the *B. pseudofirmus* OF4 *c*-ring[3,14,18] to determine whether Ala-to-Gly mutations in the AxAxAxA motif change that stability and, if so, whether such changes correlated with changes in functional capacity. Stability was probed using analyses of SDS−PAGE gels, which also revealed unanticipated changes in the mobility properties of some of the mutant *c*-rings and of *c*-monomers that dissociate from the mutant *c*-rings upon TCA treatment.

EXPERIMENTAL PROCEDURES

Bacterial Strains, Mutant Construction, and Growth Conditions. The WT strain is a derivative of alkaliphilic *B. pseudofirmus* OF4 811M that has an *Eco*RI site introduced into *atpB*.[8] Three new double mutants of the *c*-subunit, A16/18G, A18/22G, and A20/22G, were constructed as described previously for the other mutants.[8] The primers used for the mutations in this study are available upon request. Homologous recombination introduced the mutation into the chromosomal *atp* locus. Appropriate polymerase chain reaction products encompassing the *atp*

dx.doi.org/10.1021/bi2005009 |*Biochemistry* 2011, 50, 5497–5506

Table 1. Membrane Content and Function of the ATP Synthase with Different Ala-to-Gly Mutations and Stability of the Mutant *c*-Rings

			malate growth, A_{600} at 14 h (% of WT)[d]		in vitro ATP synthesis (% of WT)[e]		*c*-ring stability	
strain	β-subunit content (% of WT)[a]	OG-stimulated ATPase activity (% of WT)[c]	pH 10.5	pH 7.5	pH 10.5	pH 7.5	total *c*-subunit (% of WT)[f]	*c*-ring stability on SDS−PAGE[g]
WT	100	100	100	100	100	100	100	S
group 1, 42−51%								
A18G	51 ± 22[b]	61 ± 1[b]	65 ± 2	69 ± 2	71 ± 14	63 ± 12	69 ± 7	S
A16/18G	42 ± 10	51 ± 5	36 ± 1	50 ± 2	70 ± 1	67 ± 6	21 ± 5	VU
A16/20G	47 ± 2[b]	52 ± 10[b]	**9 ± 0.1**	46 ± 1	53 ± 10	87 ± 4	64 ± 7	VU
A16/18/20/22G	50 ± 10[b]	52 ± 14[b]	**−2 ± 1**	9 ± 1	20 ± 8[b]	81 ± 14[b]	29 ± 1	VU
group 2, 59−67%								
A16G	65 ± 6[b]	65 ± 0.4[b]	62 ± 1	84 ± 2	79 ± 3	88 ± 11	63 ± 10	U
A22G	59 ± 22[b]	77 ± 3[b]	69 ± 2	78 ± 3	ND[h]	ND[h]	95 ± 10	S
A16/20/22G	67 ± 1[b]	62 ± 9[b]	**16 ± 0.1**	38 ± 1	64 ± 7	86 ± 14	57 ± 5	VU
group 3, 76−82%								
A20G	76 ± 9[b]	72 ± 2[b]	57 ± 1	79 ± 3	ND[h]	ND[h]	79 ± 8	S
A18/22G	79 ± 5	81 ± 1	58 ± 1	77 ± 1	ND[h]	ND[h]	76 ± 5	U
A20/22G	82 ± 29	78 ± 9	57 ± 2	84 ± 0.1	72 ± 14	77 ± 6	84 ± 14	VU

[a] The amount of the ATP synthase β-subunit detected on immunoblots was quantitatively analyzed as described in Experimental Procedures. These and other values include the standard deviation. [b] The membrane levels and OG-stimulated ATPase activity of these mutants were determined in the previous study.[8] [c] The OG-stimulated ATPase activity of WT strain was 1.35 ± 0.05 units (mg of membrane protein)$^{-1}$ min^{-1}. [d] The capacity for growth on malate, expressed as the percent of WT, was assessed from the A_{600} of 2 mL cultures of strains grown for 14 h on malate-containing medium minus the A_{600} of parallel cultures of the ΔF_o mutant parent strain that is negative for nonfermentative growth.[8] [e] ATP synthesis assays were conducted on ADP- and P_i-loaded, RSO membrane vesicles from the WT and seven of the mutants, upon energization with ascorbate-PMS, as described previously.[8] During the 10 s incubation with the electron donor, the reaction mixtures were continuously aerated by vortex mixing. The WT strain had an ATP synthesis activity of 6.25 ± 1.5 and 4.44 ± 1 nmol of ATP/mg of protein at pH 7.5 and 10.5, respectively. [f] The total *c*-subunit of purified ATP synthases from each mutant, as the percent of WT, was quantified by the *c*-subunit observed via SDS−PAGE after treatment of the synthase with TCA as described in Experimental Procedures (and see Figure 3). [g] The *c*-ring stability was estimated using the following calculation: (total *c*-subunit monomer in untreated, purified ATP synthase samples/monomer in TCA-treated samples) × 100%. Three broad categories are used: S, stable (values of 3−10); U, unstable (values of 35−36); VU, very unstable (values of 60−100) (relative to a WT value of 0.5 for dissociation to monomer without TCA treatment). [h] Not determined.

operon were sequenced by Genewiz, Inc. (South Plainfield, NJ), and verified to have only the desired mutation(s). For growth experiments, the WT and mutant strains were grown on malate-containing MYE medium or on glucose-containing GYE medium at pH 7.5 and 10.5, with duplicate samples in two or three independent experiments.[8] Determinations of growth of the full mutant panel on malate, assessed by the A_{600} at 14 h in 2 mL of culture in 15 mL tubes, were conducted at the two pH values as described previously,[8] with the WT strain and the F_o deletion strain (ΔF_o, $\Delta atpB$-F) as the positive and negative controls. Appropriate dilutions were made to give A_{600} readings in the linear range of 0.3−0.5. In the earlier study that focused on the quadruple mutant, two A16/18/20/22G mutant strains were included; the mutant designated A4G-1 in the earlier study was used here for the data listed in Table 1. For several mutants, growth on MYE medium at pH 10.5 was monitored over time during growth using 50 mL of culture in 250 mL flasks, grown with shaking 250 rpm at 30 °C, in comparison with the same positive and negative controls used for the single-point growth experiments in tubes; for the growth curve experiments, the inocula for all the strains were pregrown on GYE medium at pH 10.5.

Isolation of Everted Membrane Vesicles, Assays of Their Octyl Glucoside-Stimulated ATPase Activity, and Assessment of the Membrane Content of ATP Synthase Protein. Everted membrane vesicles were prepared from the WT and three new double mutants using the protocol that was previously described.[8] The protein content for this and other experiments was determined by the method of Lowry et al.[19] OG-stimulated ATPase assays were conducted as described previously.[8] The amount of ATP synthase β-subunit found in everted membrane vesicles expressing mutant ATP synthases was compared to the amount in vesicles expressing the WT enzyme as an assessment of relative ATP synthase content of the everted vesicles. Vesicles equivalent to 1.6 μg of protein were fractionated on 11% SDS−PAGE minigels[20] and transferred electrophoretically to nitrocellulose membranes. Immunoblot analyses of the β-subunit were conducted as described in an earlier study.[8] For the purpose of quantitation, image analysis was performed using ImageJ version 1.40 (http://rsbweb.nih.gov/ij/).

Assays of ATP Synthesis by ADP- and P_i-Loaded Right-Side-Out (RSO) Membrane Vesicles. WT and mutant strains were grown to an A_{600} of 0.5−0.6 on MYE medium at 30 °C and pH 7.5 because some of the mutant strains did not exhibit significant growth at pH 10.5. Right-side-out (RSO) ADP- and P_i-loaded membrane vesicles were prepared and assayed as described in an earlier study at pH 7.5 and 10.5.[8] Briefly, the RSO vesicles were prepared and loaded with ADP and P_i in buffer at pH 8.3. Energization with 10 mM ascorbate and 0.1 mM phenazine methosulfate was initiated upon dilution of the loaded

vesicles into the assay buffer at either pH 7.5 or 10.5 at room temperature. This was followed by a 10 s reaction period, with continuous vigorous aeration, before the reactions were stopped by rapid transfer of the reaction mix to tubes with 50 μL of ice-cold 30% perchloric acid. After neutralization, the ATP content was determined by the luciferin−luciferase method.[8]

Purification of His-Tagged ATP Synthases. To facilitate the purification of the *B. pseudofirmus* OF4 ATP synthase, an 18-nucleotide sequence encoding six histidines was placed in the chromosomal *atp* operon immediately after the ATG initiation codon of the β-subunit of the ATP synthase. Briefly, a β-subunit deletion strain was first constructed via introduction of a spectinomycin cassette in place of part of *atpGD* (nucleotides 7851−8511 with *atp* operon numbering referring to the deposited sequence of the region, AF330160). Then the replaced region was reintroduced but with the additional 18-nucleotide sequence. For the construction of His-tagged mutants, a gene encoding a His-tagged β-subunit was introduced into the ΔF_o (Δ*atpB-F*) strain, and mutations were then constructed in that background in the usual way.[9]

For the expression of ATP synthase, all His-tagged strains, except for the A16/18/20/22G mutant, were cultured on MYE medium with 10% Luria-Bertani broth (1 g of tryptone, 0.5 g of yeast extract, and 1 g of NaCl per liter) at pH 7.5 rather than higher pH values because many of the mutants grew poorly on malate at pH 10.5. The A16/18/20/22G mutant was grown on glucose (pH 10.5) because of its poor malate growth at either pH 7.5 or 10.5. The growth substrate (malate vs glucose) and pH (7.5 vs 10.5) did not affect the properties of the WT *c*-ring on SDS−PAGE gels (unpublished results). Because the A16G mutant grew on malate at pH 10.5, we also checked the properties of its purified ATP synthase when the strain was grown on malate at pH 10.5. We observed no difference in either *c*-ring or *c*-monomer properties via SDS−PAGE (data not shown). Strains were grown for 4−6 h at 37 °C with 225 rpm shaking until the A_{600} reached 1.4−1.6. His-tagged ATP synthase was purified as described in detail elsewhere[5] except that cells from 12 L of culture were harvested for purification. Each strain was grown on two separate occasions, and each set was then used in a separate purification procedure. Where indicated, samples were precipitated with 10% TCA.

Purification of the *c*-Ring. The *c*-ring was partially purified as described previously.[21] Briefly, 1 mg of purified ATP synthase was mixed with 1% LS and incubated for 10 min at 65 °C. After the sample had cooled to room temperature, $(NH_4)_2SO_4$ was added to 65% saturation. The mixture was incubated for 20 min at room temperature and centrifuged for 15 min at room temperature. The supernatant was filtered through a PVDF 0.22 μm filter unit (Millipore) and dialyzed overnight against 10 mM Tris-HCl (pH 8.0) at 4 °C. The sample was concentrated on an ultra-4 5 kDa filter (Millipore). All of the samples contained the *c*-ring and the δ- and *b*-subunits.

SDS−PAGE Analyses. SDS−PAGE was conducted as described previously.[20] Proteins were visualized by silver staining.[22] A Criterion apparatus (Bio-Rad, Hercules, CA) was used for the gels shown in Figure 3, and for the gels shown in Figures 4 and 5, a larger gel (Bio-Rad Protean II) was used.

Determination of Molecular Masses of the Monomeric *c*-Subunits by MALDI-TOF-MS. Purified *B. pseudofirmus* OF4 ATP synthase (100 μL, 300−400 μg) was mixed with 1 mL of a 1:1 (v/v) chloroform/methanol mixture (CM). Phase separation was initiated by addition of 200 μL of 10 mM Tris-HCl (pH 8.0) with the *c*-subunit extracted into the organic solvent. The organic phase was evaporated using a UNIVAPO 150H vacuum concentrator (UniEquip), and the dry pellet was stored at −20 °C. For mass analysis of *c*-subunits by matrix-assisted laser desorption ionization time-of-flight mass spectrometry (MALDI-TOF-MS), the pellet was dissolved in CM and directly used for mass analysis either at the Functional Genomics Center Zürich (FGCZ) or at the Max-Planck-Institute of Biophysics.

Quantitative Analyses of *c*-Monomer Bands on SDS−PAGE Gels. Quantitative analysis of band intensity was performed using custom software. A high-resolution TIFF image of the gel was first inverted so that the protein bands appeared as bright rather than dark regions. This was followed by calculation of the average intensity in each band. In addition to these basic calculations, procedures were followed to ensure the consistency and quantitative accuracy of the comparisons. The average intensity of each band was computed over an equal area, corrected for background intensity, and normalized to a specified standard in the lane containing the protein molecular mass standards. All software for gel analysis was written in the scientific programming language Matlab (The Mathworks, Natick, MA).

Structures. The structures shown herein were created with PyMol.[23]

RESULTS

Ala-to-Gly Mutations Affect the Amount of ATP Synthase Found in the Membrane. A panel of 10 mutants (Table 1), which encompassed single, double, triple, and quadruple mutants, was used to evaluate the effects of mutations in the AxAxAxA motif of the *c*-subunit on the amount of ATP synthase found in the membrane. The ATP synthase content of membranes was assessed by β-subunit content, and the total ATPase activity was assayed under OG-stimulated conditions (OG-ATPase). The Ala-to-Gly mutations led to reductions in ATP synthase β-subunit content in everted membrane vesicles as compared to the content of WT vesicles in all strains tested except for the A20/22G mutant. The results for each of the mutants in comparison with the WT control are shown in Table 1, which divides the mutant panel into three groups based on the percent of WT β-subunit content: group 1, with 42−51%; group 2, with 59−67%; group 3, with 76−82%. No mutants with an Ala16-to-Gly change were found in group 3. The two mutants in group 3 that had the highest β-subunit contents of the mutant panel were A18/22, which had two Ala-to-Gly mutations in the alanine motif oriented toward the same neighbor subunit, and A20/22G, which had two Ala-to-Gly mutations oriented differently (Figure 1B). The total ATPase activities in the mutant versus WT vesicles were also reduced and were ≤81% of the WT value, generally correlating well with the β-subunit levels (Table 1).

Ala-to-Gly Changes in the AxAxAxA Motif Affect the Function of the ATP Synthase. The function of the ATP synthase in supporting nonfermentative growth on malate in MYE (malate yeast extract) medium was assessed for the full mutant panel in single-point experiments. For the values shown in Table 1, the A_{600} reached after growth for 14 h at pH 10.5 and 7.5 was corrected for the amount of growth exhibited by parallel cultures of the ΔF_o mutant (negative control) and compared to the WT value (Table 1); under these conditions, the WT growth was similar at pH 7.5 and 10.5. This was consistent with results obtained in earlier continuous culture experiments in which growth at pH 10.5 on malate was comparable to that at pH 7.5

in spite of a much lower proton-motive force at pH 10.5.[24] For the seven mutants that had been studied earlier, the new growth data were comparable to the prior results.[8] Many of the mutants exhibited growth deficits in malate growth at pH 10.5 relative to WT growth, but those deficits were comparable in magnitude to the deficit in membrane β-subunit content for those same mutants. Thus, for these mutants, no functional deficit could be inferred beyond that identified by reduced enzyme levels in the membrane, e.g., for the A18G, A16G, and A22G single mutants. The three mutants whose loss of nonfermentative growth capacity stood out were the A16/20G and A16/18/20/22G mutants of group 1 and the A16/20/22G mutant of group 2 (bold in Table 1), all of which exhibited a percent WT A_{600}/14 h metric that was more than 35% points lower than the percent WT β-subunit found for that mutant. For each of those mutants, the nonfermentative growth deficit observed at pH 7.5 was significantly less severe than that at pH 10.5, i.e., 46% versus 9% for A16/20G, 9% versus −2% for A16/18/20/22G, and 38% versus 16% for A16/20/22G. The three mutants in group 3 also exhibited a significant loss of nonfermentative growth capacity at pH 10.5 relative to the deficits in the β-subunit, i.e., 19−25% points lower, and exhibited no loss of nonfermentative growth capacity at pH 7.5 (Table 1). Although the data are not shown, we used the same growth protocol to obtain single-point A_{600} data for growth of the panel of mutants on GYE, glucose-containing medium, at pH 10.5 and 7.5. All the mutants exhibited glucose growth at a percent WT A_{600} that was equal to or higher than that predicted by the β-subunit content of the mutant, at pH 7.5 and 10.5.

The particularly severe defects in some of the mutants with an Ala16-to-Gly change indicated that one or more additional mutations were important determinants of the functional deficits. In addition, the severity depended upon the location of the additional mutation(s). For example, the A16G single mutant did not have a significant functional deficit relative to the percent β-subunit in the membrane, nor did the A16/18G double mutant, while the A16/20G mutant exhibited a major deficit in malate growth at pH 10.5 (Table 1). Because the two double mutants, A16/18G and A16/20G, had comparable percent β-subunit profiles, we conducted growth experiments over time in MYE medium at pH 10.5 to compare their growth phenotypes in greater detail. As shown in Figure 2, growth of the negative control, the ΔF_o strain, which could utilize only the limited fermentable components of the yeast extract that is in the MYE medium, leveled off at an A_{600} of 0.56, whereas the WT grew to an A_{600} of 1.8. The A16/18G double mutant grew at the same rate as WT after cessation of fermentative growth of the negative control, but growth of A16/18G subsequently leveled off earlier than that of WT, at an A_{600} of 1.6. Relative to the A16/18G mutant, the A16/20G mutant exhibited a deficit in both the rate of growth and its final growth point (A_{600} = 1.2). We note that the growth rates observed here during the nonfermentative growth phase were slower than those observed in earlier studies of the WT strain because the pregrowth of these cells was on glucose-containing medium, which reduces the levels of respiratory chain complexes and ATP synthase but supports comparable pregrowth of all the strains. Although not shown, we also conducted a similar set of growth experiments on single mutants A16G and A22G, whose percent β-subunit profiles were comparable. There was no significant difference in the growth rates of the two strains during the 8−11 h period of the experiment, but the level of growth of A22G after 14 h was consistently slightly higher (80% of WT growth) than that of the A16G mutant (74% of WT growth).

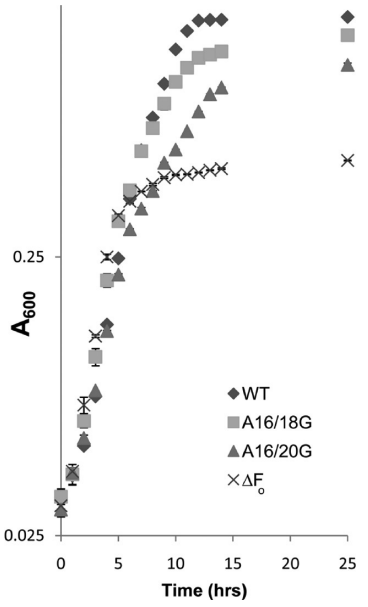

Figure 2. Comparison of the growth of the A16/18G and A16/20G mutants in malate-containing medium at pH 10.5. Growth of the two double mutants was compared to that of the WT strain and that of the ΔF_o strain, under conditions described in Experimental Procedures, with readings of the A_{600} recorded hourly for 15 h and a final point taken at 25 h.

The capacity for ATP synthesis at pH 10.5 and 7.5 was assayed in ADP- and P_i-loaded vesicles for all five mutants containing an Ala16-to-Gly mutation and at least one mutant in each of the three groups of Table 1. The same three mutants that exhibited particularly poor malate growth at pH 10.5 synthesized the least ATP at pH 10.5 in an in vitro assay in which they were compared to the WT strain. A16/20G and A16/18/20/22G of group 1 synthesized the least ATP, with 53 and 20% of the WT amount, respectively, and A16/20/22G of group 2 synthesized ATP at 64% of the WT amount; however, only the deficit in synthesis by the quadruple mutant was low compared to its percent β-subunit content in the membrane. The other mutants that were examined, single mutants A16G, A18G, and A20G and double mutant A16/18G, all synthesized ATP at 70−79% of the WT amount, values that were higher than their percent β-subunit content in some cases (Table 1).

Ala-to-Gly Change(s) in the AxAxAxA Motif Affect *c*-Ring Stability. After purification of the WT enzyme, the *c*-ring remains intact during SDS−PAGE.[5,18] Treatment of *c*-rings with TCA dissociated more than 94% of the oligomer into monomeric *c*-subunits (Figure 3A), as assessed quantitatively in lauroyl sarcosine-extracted preparations (data not shown). We used the total amount of *c*-subunit observed in TCA-treated preparations as an approximate measure of the total *c*-subunit on the gel to ascertain whether the *c*-rings of any of the mutants dissociated substantially during extraction or purification. In such instances, the total amount of *c*-subunit would be significantly lower than the WT level, although the same amount of purified ATP synthase protein was loaded on the gel for each strain. Two mutants, A16/18G and A16/18/20/22G, exhibited major reductions in the intensity of the *c*-monomer bands in the TCA-treated samples that represented loss of ~70% of the total *c*-subunit relative to the

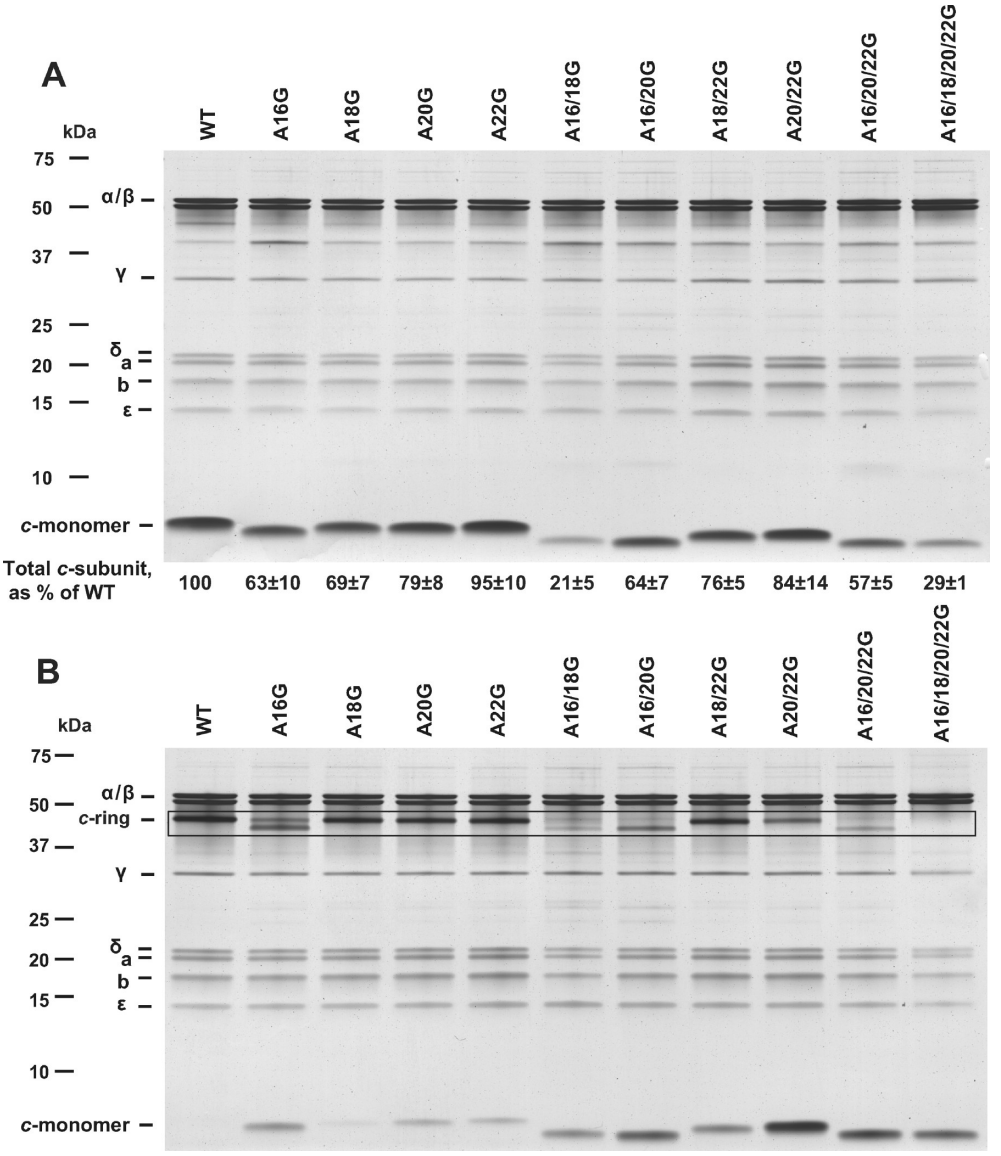

Figure 3. SDS−PAGE analyses of the purified ATP synthase from WT and mutant strains. One microgram of purified protein was loaded for each lane. The purified enzyme was resolved on 11% polyacrylamide gels and stained with silver. Samples were precipitated with TCA (A) or not treated (B); the outline in panel B highlights the *c*-ring bands. In panel A, the total *c*-subunit (as the percent of WT) that was observed via SDS−PAGE is shown under the lane. It was calculated using the equation total *c*-subunit as percent of WT = (amount of *c*-monomer in mutant TCA sample)/(amount of *c*-monomer in WT TCA sample) × 100%. The values are the average of determinations from two independent protein preparations ± the standard deviation. The intensity of the *c*-monomer was quantified by MATLAB analysis as described in Experimental Procedures.

WT amount (Figure 3A and Table 1). The A16G single mutant and A16/20/22G triple mutants, which also included an Ala16-to-Gly change, were at the low end of the remaining mutants with respect to the total amount of *c*-monomer on the SDS−PAGE gel. On the other end of the range, the A22G and A20/22G mutants exhibited total *c*-monomer contents that were close to or comparable to that of the WT preparation.

The next question addressed involved the relative amounts of *c*-monomer released by the mutants during SDS−PAGE in the absence of TCA treatment, under conditions where such release is minor or undetectable with WT preparations. Although the A16/18G and A16/18/20/22G mutants were already depleted in the *c*-subunit because of loss during extraction and purification, most of the remaining *c*-ring dissociated during SDS−PAGE. There was only very little residual *c*-ring in the A16/18G double mutant and no apparent *c*-ring remaining in the A16/18/20/22G mutant, and release of *c*-monomer clearly occurred from both these mutant preparations as well as from the triple mutant without TCA (Figure 3B). For the A16/20/22G and A16/18/20/22G mutants, there was more *c*-monomer released in samples not treated with TCA than in those treated with TCA, probably because some *c*-monomer was lost during TCA extraction. Except for the A18G single mutant, all the mutants consistently exhibited some *c*-ring dissociation in the absence of TCA treatment. Apart from the mutants that included an A16G change, the most impressive dissociation was observed in the A20/22G mutant. The stability of mutant c-rings relative to WT c-rings was estimated by an equation in footnote g of Table 1 and divided into 3 broad categories (S, stable; U, unstable; VU, very unstable). All three of the mutants containing an Ala16-to-Gly mutation that had

dx.doi.org/10.1021/bi2005009 |*Biochemistry* 2011, 50, 5497–5506

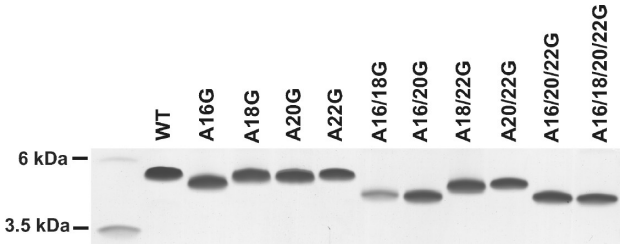

Figure 4. SDS−PAGE analyses of *c*-monomers from WT and mutant strains. The purified proteins treated with TCA were resolved on a 15% polyacrylamide gel and stained with silver as described in Experimental Procedures. The protein loaded in each lane was adjusted to give approximately comparable staining bands. The protein amount ranged from 2.5 to 7.5 μg. The gel image was cropped to show only the region of the *c*-monomer bands.

exhibited the largest functional defects, i.e., double mutant A16/20G, triple mutant A16/18/20G, and quadruple mutant A16/18/20/22G, were in the VU rotor category. However, double mutants A16/18G and A20/22G, which have much smaller functional deficits, were also in the VU category. A22G was the mutant with the most stable *c*-ring, based on both the total amount of *c*-subunit found via SDS−PAGE after TCA treatment of the samples (Table 1) and the categorization based on release of the *c*-monomer during SDS−PAGE without TCA treatment (Table 1).

Seven Ala-to-Gly Mutant *c*-Monomers Exhibit Anomalous SDS−PAGE Mobility. We observed that the *c*-subunits of some mutants ran faster on SDS−PAGE than WT *c*-subunits (Figure 3A,B). Using a large format 15% gel (see Experimental Procedures), it was possible to resolve three different sizes via SDS−PAGE (Figure 4). The apparent molecular mass of *c*-subunit monomers was determined by calibration of the gels using low-molecular mass polypeptide standards. The values for the difference between apparent molecular mass and formula molecular mass (dMW) were calculated as described by Rath et al.[25] (and see footnote [c] of Table 2). The *c*-monomers of three single mutants (A18G, A20G, and A22G) migrated almost the same as those from the WT monomer; seven mutant *c*-monomers showed a faster migration profile than the WT *c*-monomers. The *c*-subunits from the A16G, A18/22G, and A20/22G mutants ran slightly faster than the WT *c*-subunits, and those from the A16/18G, A16/20G, A16/20/22G, and A16/18/20/22G mutants migrated much faster than the WT *c*-subunits (Table 2). To verify that the *c*-subunits were intact, their masses were determined by MALDI-TOF-MS (Table 2). The measured masses all correlated with the ones calculated from the amino acid sequences of the corresponding *c*-subunit. These results indicated that all mutant *c*-subunits were intact, which excluded the possibility that some of the anomalous migration behavior of the *c*-subunits on SDS−PAGE is caused by degradation.

All Ala16-to-Gly Mutation-Containing *c*-Rings Exhibit Increased Mobility on SDS−PAGE Relative to the WT *c*-Ring. The gel patterns observed for the mutants revealed differences in *c*-ring migration compared to WT *c*-ring migration for several of them (Figure 3B). The A16/18/20/22G mutant had no clear *c*-ring band, and both the A16/18G and A16/20G double mutants and the A16/20/22G triple mutant showed weak *c*-ring bands relative to the WT *c*-ring band. The A16G single mutant exhibited two apparent bands close to where the WT *c*-ring band was observed. The upper one was at the same position of the WT band, and the other was a modestly lower band. The A16/18G and A16/20G double mutants appeared to have at least a trace of both forms. The remaining mutants, with no Ala16-to-Gly change, had *c*-ring bands in approximately the same position as the WT *c*-ring band and similar band intensities, except for the A20/22G mutant, which exhibited a lower intensity. Because of the increased mobility of *c*-ring bands in mutants containing an Ala16-to-Gly change, we used lauroyl sarcosine (LS) to extract the *c*-rings from the ATP synthase preparations purified from the WT strain and all five mutants containing the Ala16-to-Gly mutation. The LS extracts were then analyzed on large format 10% SDS−PAGE gels (Figure 5). The A16G mutant exhibited two obvious bands in the region where the WT *c*-ring was observed: a less intense band with migration comparable to that of the WT band and a more intense band below it. Trace amounts of the band comigrating with the upper A16G band were observed for the two double mutants, supporting the inference from the SDS−PAGE analyses before partial purification of the *c*-rings by LS extraction (Figure 3B). The upper band was at the same position as the WT *c*-ring, while the lower band suggested a smaller apparent size (Figure 5). The other mutants that had an Ala16-to-Gly mutation, A16/20/22G and A16/18/20/22G, exhibited single *c*-ring bands of a size comparable to those of the lower species in the A16G single mutant.

Table 2. Formula Molecular Masses, Measured Masses (MALDI-MS), Apparent Molecular Masses, and Mobility Changes of the *c*-Monomer from WT and Mutant Strains

c-monomer	formula molecular mass (Da)[a]	measured mass (Da)[b]	apparent molecular mass (Da)	mobility change (dMW, %)[c]
WT	6957	6955	5596	−19.6 ± 2.1
A16G	6943	6942	5238	−24.6 ± 2.1
A18G	6943	6942	5533	−20.3 ± 1.5
A20G	6943	6942	5549	−20 ± 1.8
A22G	6943	6942	5568	−19.8 ± 1.6
A16/18G	6929	6928	4746	−31.5 ± 1.9
A16/20G	6929	6928	4737	−31.6 ± 2
A18/22G	6929	6928	5122	−26.1 ± 1.4
A20/22G	6929	6928	5184	−25.2 ± 1.6
A16/20/22G	6915	6914	4701	−32 ± 1.5
A16/18/20/22G	6901	6904	4640	−32.8 ± 1.3

[a] Formula molecular mass estimated by Gene runner. [b] The reported masses are after subtraction of the N-terminal formylation. [c] dMW = (apparent molecular mass − formula molecular mass)/(formula molecular mass) × 100%. Values are shown ± the standard deviation. Negative values for a dMW indicate faster migration via SDS−PAGE (i.e., a lower apparent molecular mass) than expected.[25]

DISCUSSION

In this study, a panel of 10 Ala-to-Gly mutants in the AxAxAxA motif of the inner helix of the ATP synthase *c*-ring of alkaliphilic *B. pseudofirmus* OF4 was used to probe the relationship between functional effects and the number and position of the mutations. We also explored whether functional effects of the mutations correlated with changes in the physical properties of the *c*-rings that could be inferred from the behavior of the mutant enzymes or rotor-enriched fractions in SDS−PAGE analyses. A general finding was that all 10 mutations reduced the

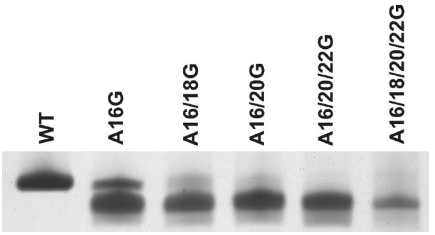

Figure 5. SDS−PAGE analyses of the *c*-rings in lauroyl sarcosine extracts of the ATP synthases from WT and mutant strains including an A16G change. The purified proteins treated with lauroyl sarcosine were resolved on a large format 10% polyacrylamide gel and stained with silver, as described in Experimental Procedures. The protein loaded in each lane was adjusted to produce bands with approximately comparable staining. The amount of protein loaded ranged from 0.5 to 1.1 μg. The gel image was cropped to show only the region of the *c*-ring bands.

amount of holoenzyme in the membrane, as assessed by the amount of membrane-associated β-subunit, and/or reduced the capacity for nonfermentative growth on malate at high pH. Another general finding was that all of the mutant *c*-rings, except for the A22G mutant *c*-ring, exhibited instability relative to the WT *c*-ring in one or both indicators of instability from the SDS−PAGE analyses (Table 1). Both GxxxG and AxxxA motifs have been proposed to stabilize helix−helix interactions in membrane proteins.[26−28] Work by Serrano et al.[29] has indicated that alanine has a stronger stabilizing effect than glycine when present in the middle of α-helices. The AxAxAxA motif of *B. pseudofirmus* OF4 is located at the interface of the inner helices of two *c*-subunits. The interaction of 13 such subunits to form a c_{13}-ring structure is mediated in part by the AxAxAxA packing motif.[14] Alanine residues at positions 16 and 20, together with the alanine residues at positions 18 and 22 from the next helix, form the hydrophobic contact area of two adjacent helices (Figure 1B). When glycine is substituted for one of the alanine residues, the contact surface is reduced and may become partially disrupted (Figure 6). This type of disruption is likely to account for the loss of stability observed here. However, although the *c*-rings of the three most functionally deficient mutants, A16/20G, A16/20/22G, and A16/18/20/22G, were in the very unstable (VU) group, the correlation between stability and function was not strong overall. For example, the A20G single mutant exhibited a significant deficit in malate growth relative to membrane β-content, whereas A22G did not; however, both mutant *c*-rings were stable (S). It appears likely that much of the stability loss among the mutants, compared to the WT strain, has an impact upon extraction of the enzyme from the membrane and/or during fractionation via SDS−PAGE but is not a property that has a major impact in vivo.

It was notable that the magnitudes of functional deficits observed in the vesicle assays of ATP synthesis were smaller than those for the same mutants in the single-point growth assays on malate at pH 10.5 (Table 1). This is likely to reflect, in part, the more vigorous aeration during the 10 s synthesis period than in the single-point growth assays in shaken tubes. The growth curve experiments conducted in flasks over time were also conducted under more highly aerated conditions than the single-point assays, and the two mutants whose growth is shown in Figure 2 exhibited a smaller growth deficit relative to the WT strain under the more aerated conditions. The ATP synthesis assays have an additional difference from malate growth assays that could result in synthesis by mutant strains that is more

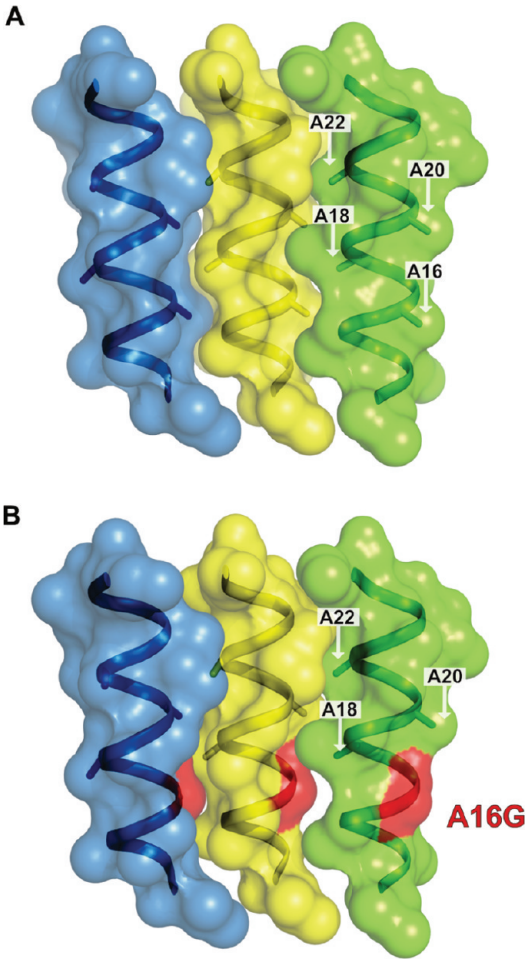

Figure 6. Model of the contact area among three inner helices of the *B. pseudofirmus* OF4 c_{13}-ring:[14] (A) WT and (B) A16G mutant. The space required for a Gly residue (G16) is smaller than that for an Ala residue (A16) with a methyl side chain, resulting in less tight and suboptimal packing with an A16G mutation in the *c*-subunit. The model is based on the structure of the c_{13}-ring (Protein Data Bank entry 2x2v). Different subunits are colored blue, yellow, and green. The A16G mutation is highlighted in red. The A16G mutation was introduced in PyMol without subsequent energy minimization or stereochemical optimization.

robust than expected from their malate growth relative to the WT strain. In the ATP synthase assays, the electron donor, ascorbate (added together with PMS), feeds directly into the proton-pumping Cta (cytochrome caa_3) cytochrome oxidase that plays a crucial role in oxidative phosphorylation by *B. pseudofirmus* OF4.[30,31] By contrast, during in vivo growth on malate, there are multiple upstream steps in electron transfer, e.g., the dehydrogenase steps, which could limit the relative rate of electron delivery. Differences in the efficacy of delivery of electrons to the respiratory chain and the availability of the final electron acceptor, oxygen, likely account for observations such as the retention by the quadruple mutant of ATP synthesis capacity (20% of WT vs its 50% of WT β-subunit content) as opposed to its failure to grow on malate at pH 10.5 (Table 1). Another striking observation of the same type is the absence of a deficit in ATP synthesis for the A16/20/22G triple mutant in the in vitro assay, relative to membrane β-content, while its growth on malate was very significantly affected at pH 10.5 and even affected at pH 7.5. The observation that an ATP synthase that

appears fully functional in the in vitro assay poorly supports malate growth highlights the complexity of in vivo OXPHOS, where issues of electron delivery, competition for protons with the antiporter(s) involved in pH homeostasis, and other challenges of this central physiological system are at play. This greater complexity may increase the sensitivity of the cells to nuanced compromises in the function of the ATP synthase that are undetected under the in vitro assay conditions.

The functional assays of the expanded mutant panel in this study clearly showed that the greatest deficits in function were found in mutants containing an Ala16-to-Gly mutation together with at least one additional Ala-to-Gly mutation. Concomitantly, SDS−PAGE analyses of purified holo-ATP synthases from the mutant panel revealed greater mobility of *c*-rings from all of the mutants containing the Ala16-to-Gly mutation. Furthermore, the A16G single mutant and to a lesser extent the double mutants in this subset also showed a minor band with the WT *c*-ring mobility that was extracted with LS along with the more mobile band. We hypothesize that the Ala16-to-Gly mutants have a c_{12}-ring but that minor amounts of a c_{13}-ring are retained in those mutants that still have at least two Ala residues of the AxAxAxA motif. A *c*-ring with a mostly c_{12}-subunit stoichiometry would account for the increased mobility. It would also be consistent with the modestly but reproducibly lower A_{600} (74% of WT growth) over 14 h reached by the A16G mutant during malate growth at pH 10.5 as compared to the A22G mutant (80% of WT growth), and the lower final A_{600} values shown in Figure 2 for both the A16/18G and A16/20G mutants compared to that of the WT strain. At the high medium pH of 10.5, the effective proton-motive force is weaker than optimal and a *c*-ring with a higher stoichiometry, which is directly related to the number of protons taken up per ATP synthesized, would support more ATP synthesis than a *c*-ring with a lower stoichiometry.[3,32] It is possible that the apparent band that retains WT mobility in some of the mutants has a c_{12} rather than the WT c_{13} stoichiometry, i.e., that the apparent c_{13}-component is an artifact. Some monomeric *c*-subunit that dissociated from the *c*-ring during purification might have stuck to a smaller c_{12}-ring to produce a ring that has the same mobility as a WT *c*-ring. Such a *c*-ring plus monomer artifact has been described in studies of the heterologously expressed *c*-subunit from the *I. tartaricus* ATP synthase.[33] However, if the alkaliphile *c*-ring is similarly sticky, it is difficult to explain why only the *c*-rings of the A16G (and perhaps, to a minor extent, A16/18G and A16/20G) mutants have the putative "stuck c_1" when other mutants release *c*-monomer but do not exhibit doublet rings. We consider it more likely that during *c*-ring assembly, a minor fraction of rings with the native c_{13} stoichiometry is formed along with the major fraction with the lower stoichiometry. The putative c_{13} fraction is formed only in strains that have A16G mutations and that retain at least two alanine residues from the AxAxAxA motif. The adequacy of two amino acid residues with side chains, in place of side chain-less glycines, to support a c_{13}-ring has precedent in the extended diameter of the c_{13}-ring of thermoalkaliphilic *C. thermarum* TA2.A1, which has two larger residues (serines) together with two glycines in the GxSxGxS sequence in the middle of its inner *c*-subunit helix (Figure 1A).[10] At present, however, the hypothesized change in *c*-subunit stoichiometry in the subset of mutants containing the A16-to-Gly mutation is strictly a hypothesis. We have not yet been able to obtain images or otherwise directly test the hypothesis that the Ala16-to-Gly mutants contain *c*-rings with a mostly or entirely c_{12} rather than the WT c_{13} stoichiometry, because of diverse technical challenges. We are continuing to seek ways to overcome these challenges.

Additional mutations in an Ala16-to-Gly background promoted dominance of the band with increased mobility, without further altering mobility (Figure 5). The results of this study show that the position(s) of the additional mutation(s) had a major effect on the functional properties of the particular mutants. For example, the A16/18G and A16/20G double mutants had *c*-rings of comparable mobility, but the functional deficits of the A16/18G mutant were significantly less severe than those of the A16/20G mutant in growth experiments (Figure 2) and ATP synthesis experiments (Table 1). Different combinations of mutations presumably affect the shape of the rings in different ways and at different depths of the ring, which could account for their different impacts on function.

Finally, we note that the monomeric *c*-subunits from seven of the mutants that were released from the *c*-rings, e.g., upon treatment with TCA, exhibited a range of increased mobility via SDS−PAGE that differed from that of the WT *c*-subunit (Figure 4). Similar behavior has been documented by others.[25,34] Rath et al.[25] concluded that the anomalous mobility of a set of mutant hairpin protein segments derived from CFTR via SDS−PAGE resulted from subtle changes in the protein folds that altered the detergent binding properties of individual mutant proteins, leading to their altered mobility. Again, the mobility change among the AxAxAxA mutants, relative to the WT mobility, was particularly pronounced in mutants with an Ala16-to-Gly change. The A16G single mutant was the only single mutant that exhibited a significant mobility change, and the multiple mutants that included an Ala16-to-Gly change were the most affected in the panel. However, the A18/22G and A20/22G mutants showed consistent indications of modestly increased mobility relative to that of the WT monomer via SDS−PAGE (Figure 4 and Table 2). It is impressive that the mutant hairpinlike *c*-subunits retain structural information in SDS−PAGE that correlates with changes in the function of the larger ATP synthase nanomachine in the complex physiological process of OXPHOS.

AUTHOR INFORMATION

Corresponding Author

*E-mail: terry.krulwich@mssm.edu. Telephone: (212) 241-7280. Fax: (212) 996-7214.

Funding Sources

This work was supported by Grants GM28454-26 (to T.A.K.), R01 HL076230 (to E.A.S.), and by P50 GM071558 (to T.A.K. and E.A.S.) from the National Institutes of Health and the Cluster of Excellence "Macromolecular Complexes" at the Goethe University Frankfurt (DFG Project EXC 115) (to T.M.) and the DFG Collaborative Research Center (SFB) 807 (to T.M.).

ACKNOWLEDGMENT

We thank Julian Langer (Max-Planck Institute of Biophysics) for the special efforts required to obtain a MALDI-TOF-MS analysis result for the A16/18/20/22G mutant *c*-subunit.

ABBREVIATIONS

CM, chloroform/methanol; DDM, dodecyl β-D-maltoside; SDS−PAGE, sodium dodecyl sulfate−polyacrylamide gel electrophoresis; dMW, difference between apparent and formula

molecular masses; DTT, dithiothreitol; LS, lauroyl sarcosine; OG, octyl β-D-glucoside; OXPHOS, oxidative phosphorylation; PMF, proton-motive force; PMSF, phenylmethanesulfonyl fluoride; TCA, trichloroacetic acid; WT, wild-type.

REFERENCES

(1) Krulwich, T. A. (1995) Alkaliphiles: 'Basic' molecular problems of pH tolerance and bioenergetics. *Mol. Microbiol. 15*, 403–410.

(2) Brändén, M., Sanden, T., Brzezinski, P., and Widengren, J. (2006) Localized proton microcircuits at the biological membrane-water interface. *Proc. Natl. Acad. Sci. U.S.A. 103*, 19766–19770.

(3) Hicks, D. B., Liu, J., Fujisawa, M., and Krulwich, T. A. (2010) F_1F_0-ATP synthases of alkaliphilic bacteria: Lessons from their adaptations. *Biochim. Biophys. Acta 1797*, 1362–1377.

(4) Mulkidjanian, A. Y., Heberle, J., and Cherepanov, D. A. (2006) Protons @ interfaces: Implications for biological energy conservation. *Biochim. Biophys. Acta 1757*, 913–930.

(5) Fujisawa, M., Fackelmayer, O., Liu, J., Krulwich, T. A., and Hicks, D. B. (2010) The ATP synthase α-subunit of extreme alkaliphiles is a distinct variant. *J. Biol. Chem. 285*, 32105–32115.

(6) Ivey, D. M., and Krulwich, T. A. (1992) Two unrelated alkaliphilic *Bacillus* species possess identical deviations in sequence from those of other prokaryotes in regions of F_0 proposed to be involved in proton translocation through the ATP synthase. *Res. Microbiol. 143*, 467–470.

(7) Krulwich, T. A., Hicks, D. B., Swartz, T. H., and Ito, M. (2007) Bioenergetic adaptations that support alkaliphily. In *Physiology and Biochemistry of Extremophiles* (Gerday, C., and Glansdorff, N., Eds.) pp 311−329, American Society for Microbiology Press, Washington, DC.

(8) Liu, J., Fujisawa, M., Hicks, D. B., and Krulwich, T. A. (2009) Characterization of the functionally critical AXAXAXA and PXXEXXP motifs of the ATP synthase *c*-subunit from an alkaliphilic *Bacillus*. *J. Biol. Chem. 284*, 8714–8725.

(9) Wang, Z., Hicks, D. B., Guffanti, A. A., Baldwin, K., and Krulwich, T. A. (2004) Replacement of amino acid sequence features of *a*- and *c*-subunits of ATP synthases of alkaliphilic *Bacillus* with the *Bacillus* consensus sequence results in defective oxidative phosphorylation and non-fermentative growth at pH 10.5. *J. Biol. Chem. 279*, 26546–26554.

(10) Matthies, D., Preiss, L., Klyszejko, A. L., Müller, D. J., Cook, G. M., Vonck, J., and Meier, T. (2009) The c_{13} ring from a thermoalkaliphilic ATP synthase reveals an extended diameter due to a special structural region. *J. Mol. Biol. 388*, 611–618.

(11) McMillan, D. G., Keis, S., Dimroth, P., and Cook, G. M. (2007) A specific adaptation in the a subunit of thermoalkaliphilic F_1F_O-ATP synthase enables ATP synthesis at high pH but not at neutral pH values. *J. Biol. Chem. 282*, 17395–17404.

(12) Arechaga, I., and Jones, P. C. (2001) The rotor in the membrane of the ATP synthase and relatives. *FEBS Lett. 494*, 1–5.

(13) Vonck, J., von Nidda, T. K., Meier, T., Matthey, U., Mills, D. J., Kühlbrandt, W., and Dimroth, P. (2002) Molecular architecture of the undecameric rotor of a bacterial Na^+-ATP synthase. *J. Mol. Biol. 321*, 307–316.

(14) Preiss, L., Yildiz, Ö., Hicks, D., Krulwich, T. A., and Meier, T. (2010) A new type of proton coordination in an F_1F_0-ATP synthase rotor ring. *PLoS Biol. 8*, e1000443.

(15) Meier, T., Polzer, P., Diederichs, K., Welte, W., and Dimroth, P. (2005) Structure of the rotor ring of F-Type Na^+-ATPase from *Ilyobacter tartaricus*. *Science 308*, 659–662.

(16) Murata, T., Yamato, I., Kakinuma, Y., Leslie, A. G., and Walker, J. E. (2005) Structure of the rotor of the V-Type Na^+-ATPase from *Enterococcus hirae*. *Science 308*, 654–659.

(17) Pogoryelov, D., Yildiz, Ö., Faraldo-Gomez, J. D., and Meier, T. (2009) High-resolution structure of the rotor ring of a proton-dependent ATP synthase. *Nat. Struct. Mol. Biol. 16*, 1068–1073.

(18) Hoffmann, J., Sokolova, L., Preiss, L., Hicks, D. B., Krulwich, T. A., Morgner, N., Wittig, I., Schägger, H., Meier, T., and Brutschy, B. (2010) ATP synthases: Cellular nanomotors characterized by LILBID mass spectrometry. *Phys. Chem. Chem. Phys. 12*, 13375–13382.

(19) Lowry, O. H., Rosebrough, N. J., Farr, A. L., and Randall, R. J. (1951) Protein measurement with the Folin phenol reagent. *J. Biol. Chem. 193*, 265–275.

(20) Schägger, H., and von Jagow, G. (1987) Tricine-sodium dodecyl sulfate-polyacrylamide gel electrophoresis for the separation of proteins in the range from 1 to 100 kDa. *Anal. Biochem. 166*, 368–379.

(21) Meier, T., Matthey, U., von Ballmoos, C., Vonck, J., Krug von Nidda, T., Kühlbrandt, W., and Dimroth, P. (2003) Evidence for structural integrity in the undecameric *c*-rings isolated from sodium ATP synthases. *J. Mol. Biol. 325*, 389–397.

(22) Nesterenko, M. V., Tilley, M., and Upton, S. J. (1994) A simple modification of Blum's silver stain method allows for 30 minute detection of proteins in polyacrylamide gels. *J. Biochem. Biophys. Methods 28*, 239–242.

(23) De Lano, W. L. (2002) *The PyMOL molecular graphics system*, DeLano Scientific, San Carlos, CA.

(24) Sturr, M. G., Guffanti, A. A., and Krulwich, T. A. (1994) Growth and bioenergetics of alkaliphilic *Bacillus firmus* OF4 in continuous culture at high pH. *J. Bacteriol. 176*, 3111–3116.

(25) Rath, A., Glibowicka, M., Nadeau, V. G., Chen, G., and Deber, C. M. (2009) Detergent binding explains anomalous SDS-PAGE migration of membrane proteins. *Proc. Natl. Acad. Sci. U.S.A. 106*, 1760–1765.

(26) Curran, A. R., and Engelman, D. M. (2003) Sequence motifs, polar interactions and conformational changes in helical membrane proteins. *Curr. Opin. Struct. Biol. 13*, 412–417.

(27) Rath, A., and Deber, C. M. (2008) Surface recognition elements of membrane protein oligomerization. *Proteins 70*, 786–793.

(28) Walters, R. F., and DeGrado, W. F. (2006) Helix-packing motifs in membrane proteins. *Proc. Natl. Acad. Sci. U.S.A. 103*, 13658–13663.

(29) Serrano, L., Neira, J. L., Sancho, J., and Fersht, A. R. (1992) Effect of alanine versus glycine in α-helices on protein stability. *Nature 356*, 453–455.

(30) Quirk, P. G., Hicks, D. B., and Krulwich, T. A. (1993) Cloning of the *cta* operon from alkaliphilic *Bacillus firmus* OF4 and characterization of the pH-regulated cytochrome *caa3* oxidase it encodes. *J. Biol. Chem. 268*, 678–685.

(31) Gilmour, R., and Krulwich, T. A. (1997) Construction and characterization of a mutant of alkaliphilic *Bacillus firmus* OF4 with a disrupted *cta* operon and purification of a novel cytochrome *bd*. *J. Bacteriol. 179*, 863–870.

(32) Meier, T., Morgner, N., Matthies, D., Pogoryelov, D., Keis, S., Cook, G. M., Dimroth, P., and Brutschy, B. (2007) A tridecameric c ring of the adenosine triphosphate (ATP) synthase from the thermoalkaliphilic *Bacillus* sp. strain TA2.A1 facilitates ATP synthesis at low electrochemical proton potential. *Mol. Microbiol. 65*, 1181–1192.

(33) Meier, T., Yu, J., Raschle, T., Henzen, F., Dimroth, P., and Müller, D. J. (2005) Structural evidence for a constant c_{11} ring stoichiometry in the sodium F-ATP synthase. *FEBS J. 272*, 5474–5483.

(34) Wehbi, H., Rath, A., Glibowicka, M., and Deber, C. M. (2007) Role of the extracellular loop in the folding of a CFTR transmembrane helical hairpin. *Biochemistry 46*, 7099–7106.